Computer Modeling in Engineering & Sciences

Tech Science Press

DOI: 10.32604/cmes.2023.025749

ARTICLE

Numerical Simulation of Low Cycle Fatigue Behavior of Ti_2AlNb Alloy Subcomponents

Yanju Wang[1], Zhenyu Zhu[2], Aixue Sha[1] and Wenfeng Hao[3,*]

[1]Materials Evaluation Center for Aeronautical and Aeroengine Application, AECC Beijing Institute of Aeronautical Materials, Beijing, 100095, China

[2]Faculty of Civil Engineering and Mechanics, Jiangsu University, Zhenjiang, 212013, China

[3]College of Mechanical Engineering, Yangzhou University, Yangzhou, 225127, China

*Corresponding Author: Wenfeng Hao. Email: hwf@yzu.edu.cn

Received: 28 July 2022 Accepted: 12 October 2022

ABSTRACT

Many titanium alloy subcomponents are subjected to fatigue loading in aerospace engineering, resulting in fatigue failure. The fatigue behavior of Ti_2AlNb alloy subcomponents was investigated based on the Seeger fatigue life theory and the improved Lemaitre damage evolution theory. Firstly, the finite element models of the standard open-hole specimen and Y-section subcomponents have been established by ABAQUS. The damage model parameters were determined by fatigue tests, and the reliability of fatigue life simulation results of the Ti_2AlNb alloy standard open-hole specimen was verified. Meanwhile, the fatigue life of Ti_2AlNb alloy Y-section subcomponents was predicted. Under the same initial conditions, the average error of fatigue life predicted by two different models was 20.6%. Finally, the effects of loading amplitude, temperature, and Y-interface angle on fatigue properties of Ti_2AlNb Y-section subcomponents were investigated. These results provide a new idea for evaluating the fatigue life of various Ti_2AlNb alloy subcomponents.

KEYWORDS

Fatigue life prediction; stiffness degeneration; Ti_2AlNb alloy; continuous damage mechanics; numerical simulation

1 Introduction

Advances in the aerospace industry require new lightweight materials and complex integral component forming technologies to improve fuel efficiency and payloads. Ti_2AlNb alloy has good plasticity and fracture toughness at room temperature, creep and fatigue resistance at a high temperature, high Young's modulus, and specific strength. Compared with the traditional high-temperature titanium alloy, the upper limit of application temperature of Ti_2AlNb alloy exceeds 600°C and reaches 650°C∼700°C [1–4].

Many titanium alloy subcomponents are subjected to fatigue loading in aerospace engineering, resulting in fatigue failure. The fatigue behavior of Ti_2AlNb alloy subcomponents is fundamental. The fatigue properties of Ti_2AlNb alloy were mainly studied by analyzing the influence of microstructure,

alloy composition and surface treatment. Through the study of the Orthorhombic structure (O phase), the formation mechanism of Ti_2AlNb alloy is diverse and complex, and the formation of the material is strongly dependent on the thermal machining process [5–8]. When the O phase layer is thick, the longer the slip path, the lower the fatigue life. The thin O phase layer and the dense O/B2 phase interface can improve the fatigue crack initiation resistance. By adjusting the ratio of Al/Nb or adding alloying elements, such as Mo, Zr, Fe, Ta, W, Si and V, the mechanical properties of Ti_2AlNb alloy, such as strength, plasticity, oxidation resistance and creep resistance, have been significantly changed [9–12]. For instance, W effectively improves the high temperature tensile strength of Ti_2AlNb alloy from 752 to 1123 MPa [13]. Zhang et al. [14,15] studied the effect of cooling rate on the microstructure and tensile properties of Ti_2AlNb alloy. Chen et al. [16] studied the effect of shot peening on the fatigue performance of Ti_2AlNb. They measured the residual stress of the specimen after glass fine shot peening by X-ray diffraction and electropolishing. Based on the image crystal plasticity model, Fu et al. [17] studied the influence of size and distribution for the O phase on the fracture properties of Ti_2AlNb superalloy. After shot peening, residual compressive stress was introduced into the surfaces of samples, which offset part of the tensile stress, delayed the initiation and propagation of cracks, and significantly increased the fatigue strength limit from 170 to 360 MPa and the high cycle fatigue life is prolonged more than 25 times [16,18]. The study of fatigue properties and deformation behaviour of Ti_2AlNb alloy focuses on the material parts, and the fatigue behavior of subcomponents needs further study.

The fatigue life prediction of titanium alloy can be divided into three main criteria: stress criteria [19,20], energy criteria [21–23] and strain criteria [24–26]. The stress criterion is suitable for the life prediction of High Cycle Fatigue (HCF). The energy criterion considers that material damage accumulates strain energy caused by stress. When the energy reaches the critical value, the material will fail, and it cannot reflect the difference in the influence of various stress (strain) components on the material failure. The strain criterion of Morrow et al. [22] has been widely applied to the fatigue life prediction of elastic-plastic materials under Low Cycle Fatigue (LCF). Based on the strain criterion, Bäumel et al. [27] first found that a uniform description of fatigue parameters of different types of metal materials would lead to errors, so fatigue parameter expressions of steel, titanium and aluminium were given respectively. Seeger theory general slope method has significant advantages in the fatigue life prediction of titanium alloys. Continuum Damage Mechanics (CDM) has been rapidly developed and applied in recent years. CDM theory connects fatigue with microcrack evolution and further develops the traditional fatigue theory [28–31]. Compared with the classical fatigue theory, CDM theory is more consistent with the microscopic mechanism of the fatigue process observed in the experiments. The damage variable can measure the fatigue damage process more directly, which is convenient for considering the fatigue damage. Zhou et al. [32,33] improved the Lemaitre damage evolution model and applied the CDM method to fatigue damage and life prediction of titanium alloy TC4 materials and components, achieving excellent accuracy.

To sum up, the fatigue behavior of Ti_2AlNb alloy subcomponents is still an open question. Seeger fatigue life theory and the improved Lemaitre damage evolution theory are used to predicting the fatigue life of Ti_2AlNb alloy standard open-hole specimen and Y-section subcomponents. The research method has a particular reference significance for predicting the fatigue life of Ti_2AlNb alloy subcomponents and provides a new idea for evaluating the fatigue life of various engineering structures.

2 Methodology

2.1 Seeger Theory

Seeger theory has been widely used to estimate the elastic-plastic stress and strain of notched parts under uniaxial or multiaxial stress (monotone and cyclic loading). Its accuracy has also been verified in relevant experiments [34].

$$\varepsilon = \frac{\sigma}{E} + \left(\frac{\sigma}{K'}\right)^{\frac{1}{n'}} \tag{1}$$

where K' is the strain hardening coefficient, and n' is the strain hardening exponent.

The relation between the real local stress amplitude and durability is:

$$\frac{\Delta\sigma}{2} = \sigma_f^{'}\left(2N_f\right)^b \tag{2}$$

where b is the fatigue strength exponent (Basquin's exponent), $\sigma_f^{'}$ is the fatigue strength coefficient and N_f is the number of cycles to failure.

The true fracture strength (or stress) is shown to be:

$$\sigma_f = \frac{P_f}{A_f} \tag{3}$$

where P_f is the load at fracture, and A_f is the cross-sectional area at fracture.

The fatigue ductility coefficient, $\varepsilon_f^{'}$, is approximately equal to the true fracture ductility ε_f. The true fracture ductility was shown to be:

$$\varepsilon_f = ln\left(\frac{A_0}{A_f}\right) \tag{4}$$

where A_0 is the original cross-sectional area.

Fatigue life can also be approximated by Eq. (5).

$$2N_f = \left(\frac{\varepsilon_f^{'}E}{\sigma_f^{'}}\right)^{\frac{1}{b-c}} \tag{5}$$

The fatigue strength exponent will usually be between -0.05 and -0.12. The fatigue ductility exponent, c, will usually be between -0.5 and -0.7.

From Eqs. (1) and (2), the following relation can be deduced:

$$K' = \frac{\sigma_f^{'}}{\left(\varepsilon_f^{'}\right)^{n'}} \tag{6}$$

$$n' = \frac{b}{c} \tag{7}$$

Seeger theory involves fatigue parameters as shown in Table 1, $a = 1.0$ when σ_b/E is less than 0.003, otherwise $a = 1.375 - 125\sigma_b/E$. σ_b is tensile strength.

2.2 The Improved Lemaitre Damage Evolution Theory

In the framework of CDM, damage is defined as the development of pores in microscopic, submicroscopic, and macroscopic fracture processes of materials, which is accompanied by the deterioration of the mechanical properties of materials. The 'damage' does not correspond to the actual

crack. In metallic materials, the damage usually has no directivity, called isotropic damage, and can be expressed as a scalar quantity.

Table 1: Seeger theoretical method fatigue parameters of titanium alloy

σ_f'	ε_f'	b	c	n'	K'
$1.67\sigma_u$	0.35	−0.095	−0.69	0.11	$1.61\sigma_u$

According to the equivalent strain hypothesis proposed by Lemaitre and Desmorat, the effective stress acting on the effective area can be defined as:

$$\widetilde{\sigma}_{ij} = \frac{\sigma_{ij}}{1-D} \tag{8}$$

where σ_{ij} is the nominal stress, without considering the influence of damage, D is the damage variable.

According to the constitutive damage model proposed by Krajcinovic and Lemaitre, the fatigue damage of metal materials in LCF is mainly caused by accumulated plastic strain. The greater the cumulative plastic deformation, the more excellent the energy dissipation caused by damage.

Damage increment, $\dot{D}$, can be expressed as:

$$\dot{D} = \frac{Y}{S}\dot{p} \tag{9}$$

Damage strain energy release rate, Y, can be expressed as:

$$Y = \frac{\sigma_{eq}^2 R_V}{2E\,(1-D)^2} \tag{10}$$

where S is material constant, $\dot{p}$ is cumulative plastic strain increment, σ_{eq} is Von Mises stress, and R_V is stress triaxiality. In uniaxial state, R_V is 1.

Substitute Eq. (10) into Eq. (9)

$$\dot{D} = \frac{\sigma_{eq}^2 R_V}{2ES\,(1-D)^2}\dot{p} \tag{11}$$

According to the study of Zhou et al. [32], Eq. (11) cannot sufficiently describe the phenomenon of a sharp increase in damage of titanium alloy materials before failure. Eq. (11) is improved as:

$$\dot{D} = \frac{\sigma_{eq}^2 R_V}{2ES\,(1-D)^{\alpha}\,(1-D/D_c)}\dot{p} \tag{12}$$

where α is the material constant, and D_c is damage limit.

For the LCF behavior of metal materials, the Ramberg-Osgood cycle is usually adopted. Within a stable cycle, the plastic strain can be expressed as:

$$\frac{\Delta p}{2} = \left(\frac{\Delta\sigma_{eq}}{2K\,(1-D)}\right)^{1/n} \tag{13}$$

where Δp is the change of cumulative plastic strain in a cycle, K is the cyclic strengthening coefficient, n is the cyclic strain hardening exponent.

The equivalent stress difference, $\Delta\sigma_{eq}$, can be expressed as:

$$\Delta\sigma_{eq} = \Delta\sigma_{eq}^{'} - \Delta\sigma_{eq}^{''} < \sigma_{m}^{''} > \tag{14}$$

where $\Delta\sigma_{eq}^{'}$ is the peak equivalent stress, $\Delta\sigma_{eq}^{''}$ is the valley equivalent stress, $\sigma_{m}^{''}$ is the average stress.

Assuming that the damage changes very little in a cycle, it can be approximated that the damage variable D in Eq. (13) is a specific value. By differentiating both ends of Eq. (13), the plastic strain rate can be obtained:

$$dp = \frac{1}{nK\left(1-D\right)}\left(\frac{\sigma_{eq}}{K\left(1-D\right)}\right)^{\frac{1}{n}-1} d\sigma_{eq} \tag{15}$$

By using the established damage constitutive relation Eqs. (13), (15), and damage evolution Eq. (12), the change process of D at any point in the whole fatigue process can be theoretically given through numerical analysis. When D reaches D_c at the danger point, fatigue failure occurs in the subcomponents, which can be expressed as follows:

$$\int_0^{N_f} \frac{\delta D}{\delta N} dN = D_c \tag{16}$$

where $\frac{\delta D}{\delta N}$ is the damage increment within a cycle.

In order to calculate $\frac{\delta D}{\delta N}$ quickly and accurately, the following two assumptions are proposed:

A. Within a cycle, the damage changes, ΔD, very little, and D can be approximated as a constant;
B. When D_c is small, D is a small quantity, so the stress field variation between different cycles can be ignored.

By differentiating both ends of Eq. (12):

$$dD = \frac{\sigma_{eq}^2 R_V}{2ES\left(1-D\right)^{\alpha}\left(1-D/D_c\right)} dp \tag{17}$$

For symmetric fatigue cycles, the hysteresis loop is central symmetry:

$$\frac{\delta D}{\delta N} = \oint dD = \int_A^B dD + \int_B^A dD = 2\int_A^B dD \tag{18}$$

By substituting Eqs. (14), (15) and (17) into Eq. (18) and integrating them, the fatigue damage within a cycle can be obtained, that is, the cumulative damage of Ti_2AlNb alloy in each loading cycle is:

$$\frac{\delta D}{\delta N} = \frac{\left(\Delta\sigma_{eq}/2\right)^{2+1/n} R_V}{ES\left(K\right)^{1/n}\left(1-D\right)^{\alpha+1/n}\left(1-D/D_c\right)\left(1+2n\right)} \tag{19}$$

where S is a variable mainly related to $\Delta\sigma_{eq}$:

$$S = Ae^{\left(B\frac{\Delta\sigma_{eq}}{2}\right)} \tag{20}$$

Material parameters involved in the damage model are shown in Table 2 [35].

Table 2: Damage parameters of Ti_2AlNb alloy

A	B	K	n	α	D_c
77.62	0.0023	2104	0.133	4.1	0.06

2.3 Material Parameters of Ti_2AlNb Alloy

2.3.1 Young's Modulus and Poisson's Ratio

In order to measure the Elastic modulus and Poisson's ratio of Ti_2AlNb alloy, the bar specimens were tested using the dynamic (acoustic resonance) method according to ASTM E1875-20. The data required for the excerpt is shown in Table 3.

Table 3: Elastic modulus, shear modulus and Poisson's ratio of Ti_2AlNb alloy

Temperature, T(°C)	E(GPa)	G(GPa)	ν
24	113.2	43.5	0.301
500	103.7	39.5	0.313
600	99.7	37.9	0.315
700	95.0	36.1	0.316

2.3.2 High Temperature Fatigue Tests of Standard Open-Hole Specimens

As the operating temperature range of Ti_2AlNb alloy subcomponents includes 500°C∼700°C, the standard open-hole specimen was selected for the test, as shown in Fig. 1. The machine used in high temperature tensile test is shown in Fig. 2. The results of the static tensile test are shown in Fig. 3, the tensile strength of 550°C and 650°C is 990 and 908 MPa, respectively. The machine used in high temperature fatigue tensile test is shown in Fig. 4. The fatigue test results are shown in Table 4, where R is stress ratio, F is the maximum tensile force, ε is the maximum strain, and N_f is fatigue life. In this paper, the LCF life of subcomponents is mainly studied. Therefore, the failure cycles of Ti_2AlNb alloy standard open-hole specimens are all lower than 10^4.

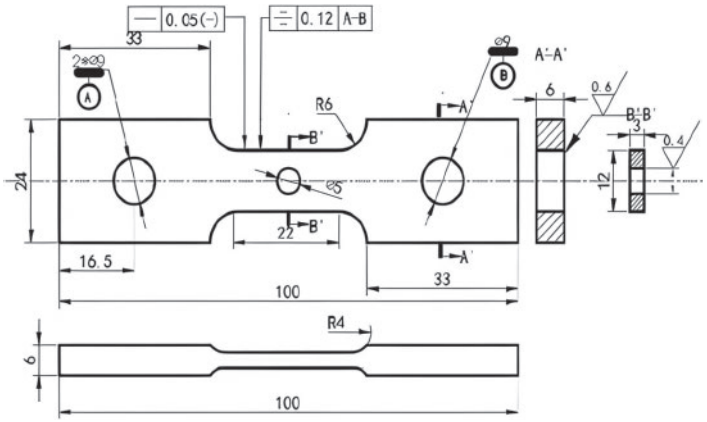

Figure 1: The size of Ti_2AlNb alloy standard open-hole specimen

Figure 2: High temperature tensile testing machine (Tinius Olsen 100ST)

3 Numerical Simulations of Ti_2AlNb Alloy Subcomponents

Numerical methods to simulate the behavior of materials can reduce the design and experimental costs, and the combination of experimental and simulated data is more consistent with the actual situation [36]. Firstly, the finite element model (FEM) of Ti_2AlNb alloy standard open-hole specimens were analyzed for grid convergence. Then, the fatigue life of Ti_2AlNb alloy standard open-hole specimens was predicted. The reliability of the two theoretical methods was analyzed and the fatigue parameters were determined. Finally, the two theoretical methods were used to predict the fatigue life of Ti_2AlNb alloy Y-section subcomponents.

3.1 Mesh Size of Standard Open-Hole Specimens

The FEM model of Ti_2AlNb alloy standard open-hole specimen was established in ABAQUS software. Three-dimensional four-node linear solid elements (C3D4) were used in the model. The element is defined by four nodes with three degrees of freedom for each node: translations in the nodal directions, x, y and z. To accurately obtain the local stress field of the specimen under cyclic loading, high-quality mesh discretization is needed [37].

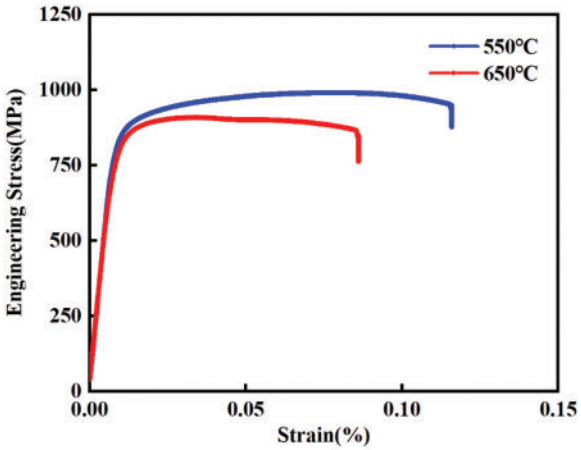

Figure 3: Tensile stress-strain curve

Figure 4: High temperature fatigue tensile testing machine (Instron 8801)

Table 4: Fatigue test data of Ti_2AlNb alloy standard open-hole specimen

T(°C)	R	F(kN)	ε(%)	N_f
550	−1	12.84	1.353	492
		10.52	1.057	1357
		9.25	0.931	2467
		7.16	0.718	5298
		6.73	0.592	7627
650	−1	8.56	0.992	714
		7.75	0.668	1861
		6.41	0.616	3634
		6.05	0.583	6923

The convergence solution independent of the mesh size is obtained in the numerical calculation after the mesh sensitivity analysis, as shown in Fig. 5. When the global mesh size (GS) is 2 mm, and the local mesh size (LS) is 0.2 mm, the numerical calculation accuracy and calculation time are the best for the Seeger fatigue life theory. A total of 31,765 elements are created, as shown in Fig. 6a. When the GS is 2 mm, and the LS is 1 mm, the numerical calculation accuracy and calculation time are the best for the improved Lemaitre damage evolution theory. A total of 15,265 elements are created, as shown in Fig. 6b.

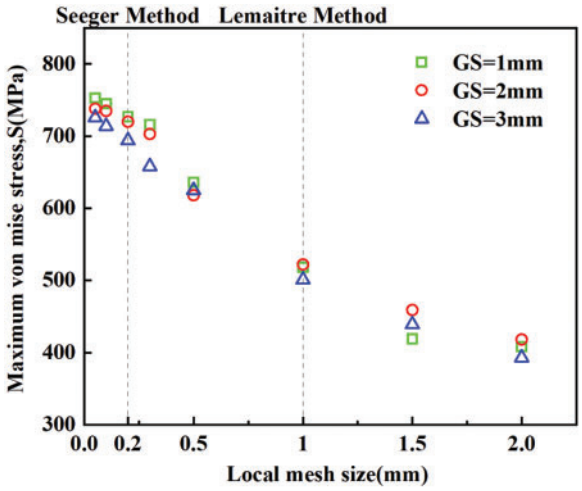

Figure 5: Scatter diagrams of trend of solution convergence of Ti_2AlNb alloy standard open-hole specimens model based on mesh size (Initial conditions: $T = 550°C$, $F = 7.16$ kN)

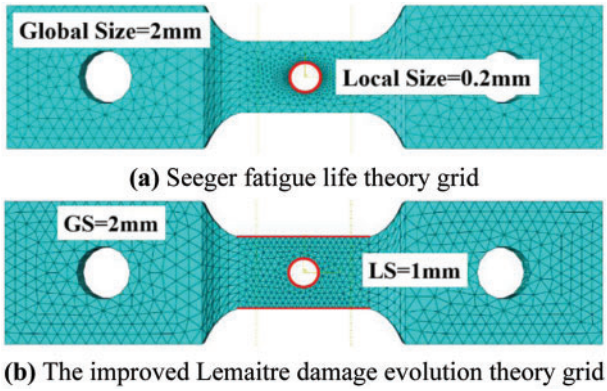

Figure 6: Grid size of Ti_2AlNb alloy standard open-hole specimen

Seeger method is to directly predict the fatigue life through empirical formulas based on the stress calculation results, so selecting finer grid elements is useful to improve the accuracy. The improved Lemaitre method calculates the cumulative damage according to the average stress of the grid. If the grid elements are selected too fine, the grid stiffness at the stress concentration will degrade rapidly until failure, leading to a large error in the predicted fatigue life. Therefore, selecting an appropriate grid element density can reduce the error.

3.2 Predicting Fatigue Life of Standard Open-Hole Specimen by Seeger Theory

Based on Seeger fatigue life theory, the static tensile results of the Ti_2AlNb alloy standard open-hole specimen of FEM were post-processed in FE-SAFE software. The fatigue cloud diagram of the FEM was generated, and showed the predicted fatigue life of a finite element structure at different positions. According to Fig. 7a, when $F = 12.84$ kN, the fatigue life of the most dangerous point $N_f = 10^{2.782}$, that is, failure after 605 cycles. According to Fig. 7b, when $F = 6.73$ kN, the fatigue life of the most dangerous point $N_f = 10^{3.908}$, that is, failure after 8,090 cycles.

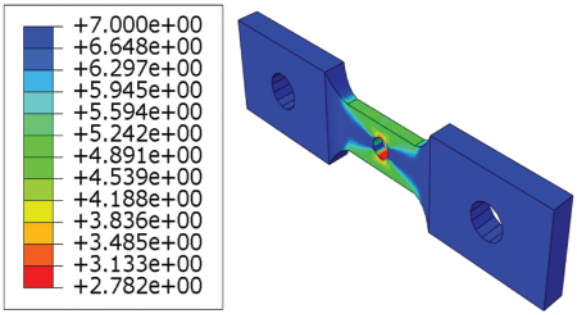

(a) Initial conditions: T=550°C, F=12.84 kN

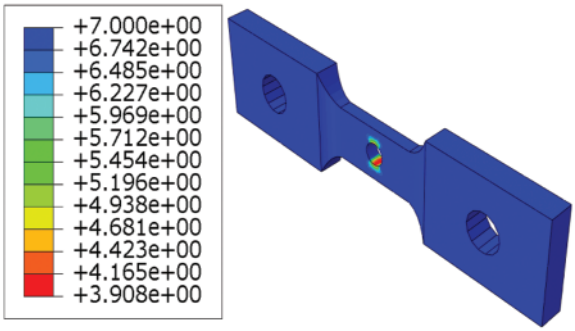

(b) Initial conditions: T=550°C, F=6.73 kN

Figure 7: Seeger theoretical fatigue life cloud diagram of Ti_2AlNb alloy standard open-hole specimens

Seeger theoretical error w_{Seeger} calculation formula is introduced:

$$w_{Seeger} = \frac{\left|N_{f-Seeger} - N_{f-Test}\right|}{N_{f-Test}} \times 100\% \tag{21}$$

where $N_{f-Seeger}$ is the maximum failure cycle number of Seeger theory, and N_{f-Test} is the maximum failure cycle number of tests. The maximum number of failure cycles is the number of cycles a subcomponent undergoes when it fails ($D = D_c$) under periodic load.

The fatigue life of Ti_2AlNb alloy standard open-hole specimens was calculated at 550°C under five different forces: 12.84, 10.52, 9.25, 7.16 and 6.73 kN. When the temperature is 650°C, the fatigue life was calculated under five forces: 8.56, 7.75, 6.41 and 6.05 kN. Seeger fatigue life prediction value (Seeger) and test fatigue life value (Test) are summarized, as shown in Fig. 8. Eq. (21) is used for error analysis when the initial conditions are identical. The average error of maximum failure cycles at 550°C and 650°C is 12.4% and 15.2%, respectively. The nine-point average error between the Seeger theory and the test value is 13.8%.

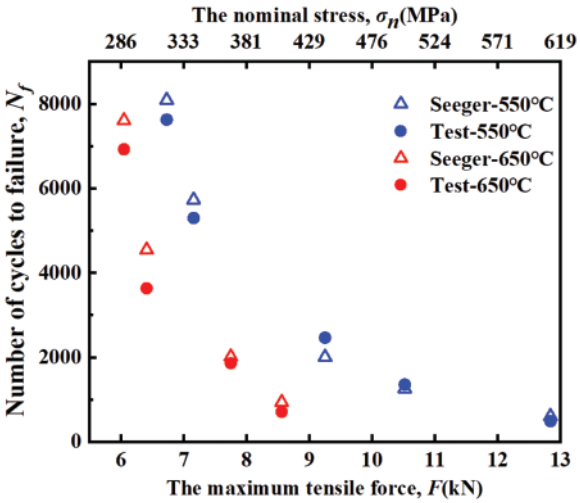

Figure 8: Scatter diagrams of Seeger theoretical fatigue life and test fatigue life of Ti_2AlNb alloy standard open-hole specimens

Although Seeger theory can predict the fatigue life of Ti_2AlNb alloy specimens within the allowable error range, there are still some defects. Seeger theory gives fatigue parameters based on many fatigue tests of Al-Ti alloy. Still, it is not rigorous enough to adopt uniform titanium alloy parameters for Ti_2AlNb alloy. Seeger theory read the equivalent stress of all grids in a static tensile process of the FEM. It calculates the fatigue life by using titanium alloy's approximate fatigue life formula, which could not show the complete stiffness degradation process.

3.3 Predicting Fatigue Life of Standard Open-Hole Specimen by the Improved Lemaitre Theory

The FEM of Ti_2AlNb alloy standard open-hole specimen is subjected to axial loads on both cross-sections. The periodic, constant amplitude load adopts the loading method of the triangular wave, and each analysis step carries out a complete tension and compression process. The specific amplitude is shown in Fig. 9.

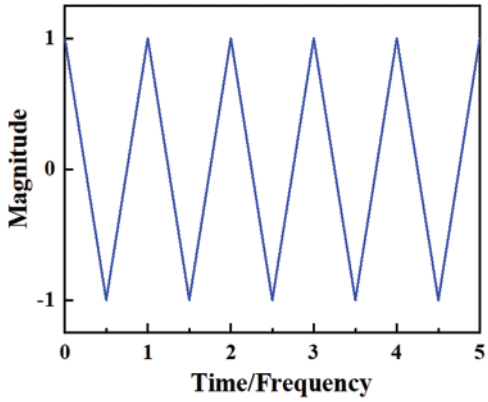

Figure 9: The smooth analysis step periodic triangular wave load

The improved Lemaitre damage evolution theory is coupled to ABAQUS through the UMAT subroutine to simulate the low cycle fatigue damage of Ti_2AlNb alloy standard open-hole specimen. Firstly, the stress-strain field is calculated, and then the damage of elements is calculated according to the global element stress. With the increase in the number of cycles, the damage to elements accumulates continuously. When the damage of elements reaches critical damage ($D_c = 0.06$), the element fails and loses its load-carrying capacity. The specific process is shown in Fig. 10. The maximum number of failure cycles equals the total analysis step time multiplied by the number of loading cycles per analysis step.

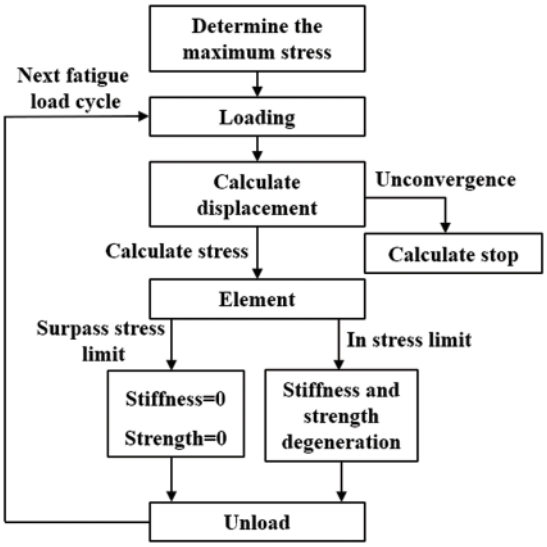

Figure 10: Flow chart of fatigue life calculated by the improved Lemaitre theory

When the initial condition is $T = 550°C$ and $F = 12.84$ kN, Fig. 11 shows the fatigue damage process of Ti_2AlNb alloy standard open-hole specimen under cyclic loading. Figs. 11a–11c show fatigue damage accumulation, and Figs. 11d–11e show the rapid expansion of fatigue damage.

The error of the improved Lemaitre damage evolution theory $w_{Lemaitre}$ is introduced:

$$w_{Lemaitre} = \frac{\left|N_{f-Lemaitre} - N_{f-Test}\right|}{N_{f-Test}} \times 100\% \tag{22}$$

where $N_{f-Lemaitre}$ is the maximum number of failure cycles of the improved Lemaitre damage evolution theory.

The improved Lemaitre prediction value (Lemaitre) and test fatigue life value (Test) are summarized, as shown in Fig. 12. Eq. (22) is used for error analysis when the initial conditions are identical. The average error of maximum failure cycles at 550°C and 650°C is 21.4% and 12.5%, respectively. The stiffness of the grid element degrades rapidly when the cyclic stress is high, resulting in a significant error at 550°C. The nine-point average error between the improved Lemaitre theory and the Test value is 16.9%.

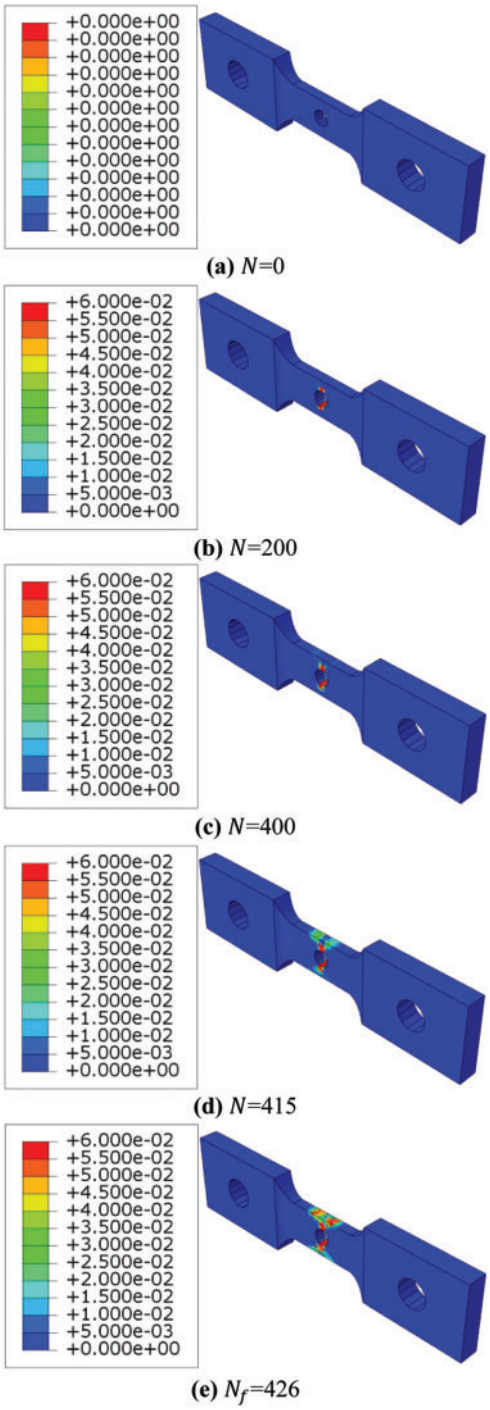

Figure 11: Damage evolution of Ti_2AlNb alloy standard open-hole specimen (Initial conditions: $T =$ 550°C, $F = 12.84$ kN)

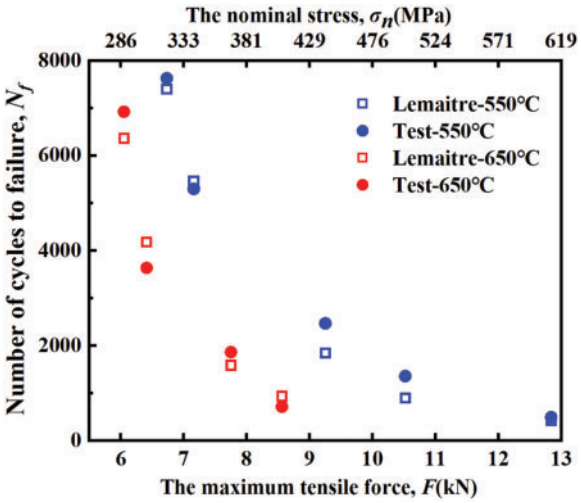

Figure 12: Scatter diagrams of the improved Lemaitre theoretical fatigue life and Test fatigue life of Ti_2AlNb alloy standard open-hole specimens

The difference between Seeger theory method and the improved Lemaitre damage evolution theory in predicting the fatigue life of structural parts can be understood through the simulation in 3.2 and 3.3. The advantage of Seeger method is that it can quickly predict the fatigue life of structural parts through empirical formulas by using the stress calculation results. The disadvantage is that it cannot show the damaging effect of fatigue load on structural parts. The advantage of the improved Lemaitre method is that it can fully show the damage process of fatigue load on structural parts, while the disadvantage is that it needs a long calculation time. The UMAT subroutine must be modified when different metal materials are switched.

3.4 Predicting Fatigue Life of Y-Section Subcomponents

For feature extraction of structural parts of integral investment casting casing of Ti_2AlNb alloy, there are many Y-shaped areas with three interface interactions in the casing section, as shown in Fig. 13. According to this characteristic, the fatigue properties of the simulated subcomponents were tested at the interface angles of 30°, 40° and 60°, respectively. The fatigue properties of the subcomponents with different interface angles were compared and analyzed. Fig. 14 shows the dimensions of the three Y-section subcomponents.

The fatigue life of the Ti_2AlNb alloy Y-section subcomponents with the interface angle of 30° was calculated under five different loads: 22, 20, 18, 16 and 14 kN. The fatigue life of the Y-section subcomponents with the angle of 40° was calculated under five loads: 20, 18, 16, 14 and 12 kN. The fatigue life of the Y-section subcomponents with the angle of 60° was calculated under five loads: 18, 16, 14, 12 and 10 kN. Fatigue life values predicted by Seeger theory (Seeger) and fatigue life values predicted by the improved Lemaitre damage evolution theory (Lemaitre) are summarized, as shown in Fig. 15.

The error between Seeger and the improved Lemaitre method, w_Y, is introduced:

$$w_Y = \frac{\left|N_{f-Seeger} - N_{f-Lemaitre}\right|}{N_{f-Lemaitre}} \times 100\% \tag{23}$$

When the initial conditions are identical, Eq. (23) is used to analyze the predicted life values of the two fatigue theories. At 550°C, the average errors of the maximum failure cycles of Y-section subcomponents are 15.1%, 25.0% and 15.4% when the angle of the interface area is 30°, 40° and 60°, respectively. At 650°C, the average errors are 19.8%, 26.8% and 21.6% when the angle is 30°, 40° and 60°, respectively.

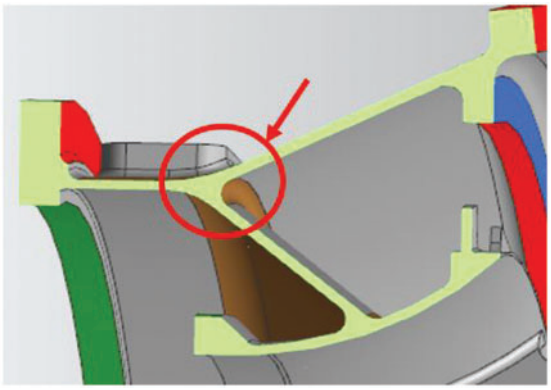

Figure 13: Y-shaped area of aviation components

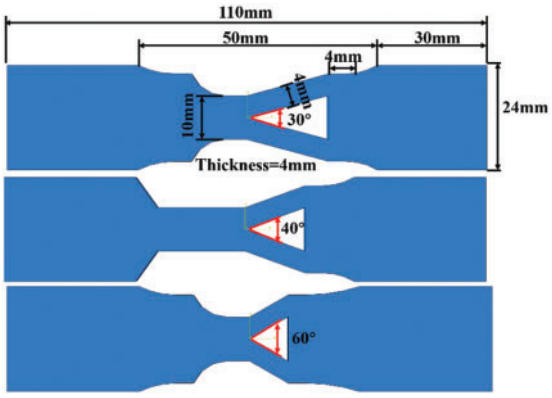

Figure 14: Dimension drawings of three Y-section subcomponents

Fig. 15 shows that when the maximum failure cycles are identical, the periodic loads carried by Ti_2AlNb alloy Y-section subcomponents at 650°C are all smaller than those carried at 550°C. Temperature is negatively correlated with the fatigue life of the subcomponents. When the temperature is constant, decreasing the load amplitude will increase the number of failure cycles of Ti_2AlNb alloy Y-section subcomponents. The load amplitude is negatively correlated with the fatigue life of the subcomponents.

The effect of interface angle on the fatigue life of Ti_2AlNb alloy Y-section subcomponents is studied by two theoretical methods. When the initial conditions are $T = 550$°C and $F = 14$ kN, Seeger theoretical fatigue life cloud diagrams of the three subcomponents are observed, as shown in Fig. 16. When the interface angle is 30°, 40° and 60°, the maximum failure cycles are 3047, 1896 and 706, respectively. The larger the interface angle, the smaller the fatigue life. When the initial conditions are $T = 550$°C and $F = 14$ kN, the stiffness degeneration process of Ti_2AlNb alloy Y-section subcomponents at different interface angles is shown in Figs. 17–19, respectively. By observing the failure position of the structures, it is found that the increase of the angle of the interface area will amplify the stress concentration effect, thus reducing the fatigue life, which is consistent with the Seeger theory results.

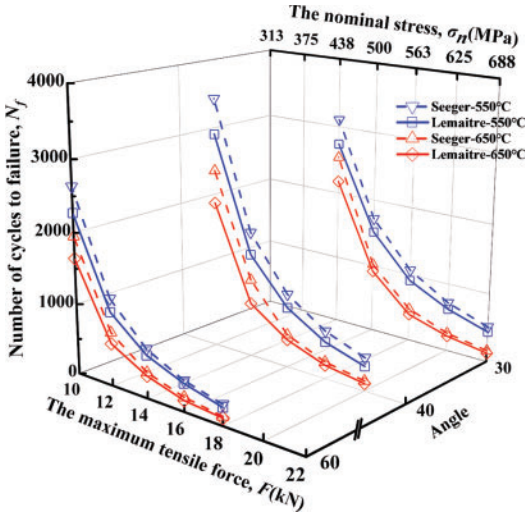

Figure 15: The maximum failure cycles of Ti_2AlNb alloy Y-section subcomponents at different interface angles, loads and temperatures

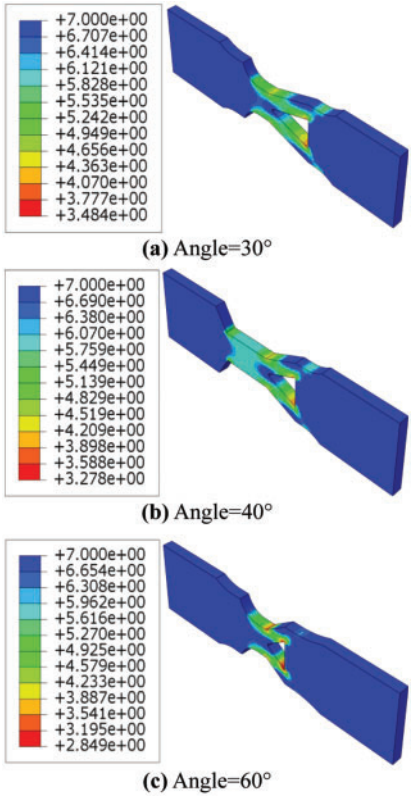

Figure 16: Seeger theoretical fatigue life cloud diagram of Ti_2AlNb alloy Y-section subcomponents (Initial conditions: $T = 550$°C, $F = 14$ kN)

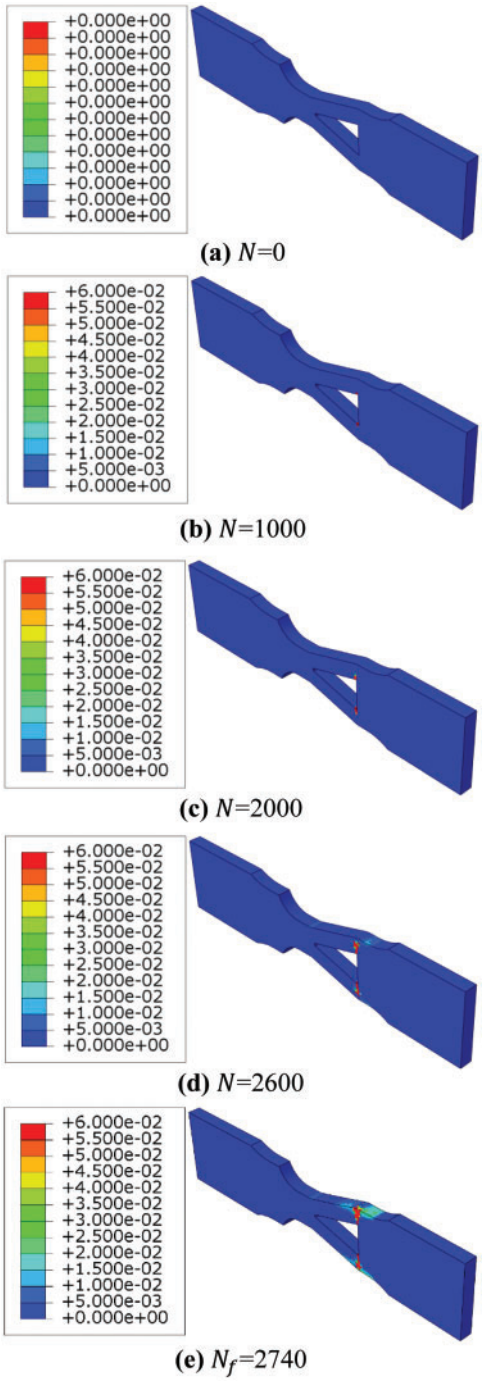

Figure 17: Damage evolution of Ti_2AlNb alloy 30° Y-section subcomponents (Initial conditions: $T =$ 550°C, $F = 14$ kN)

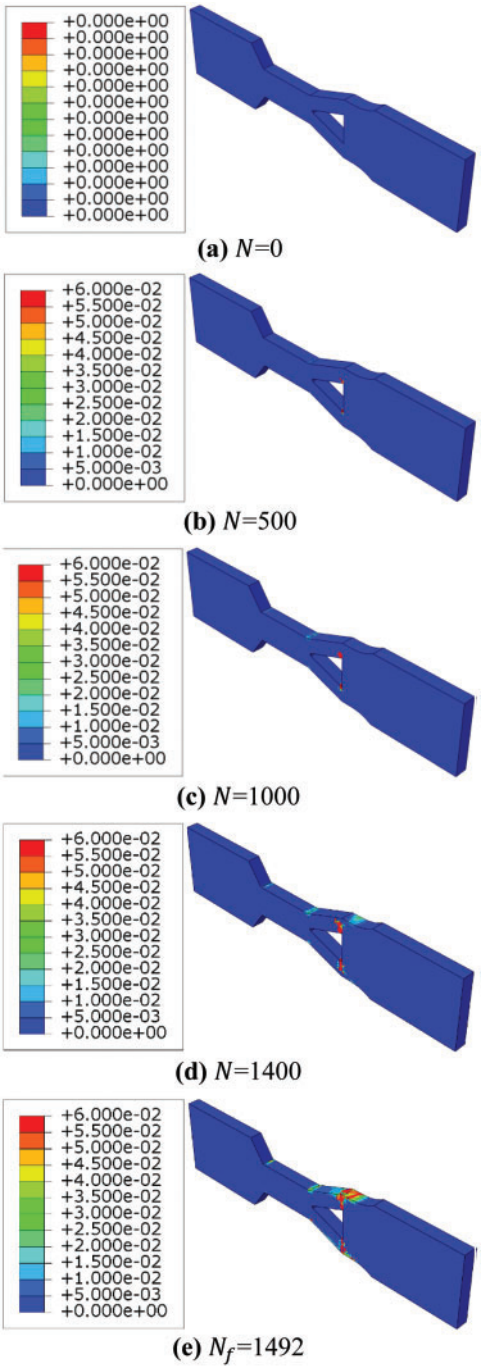

Figure 18: Damage evolution of Ti_2AlNb alloy 40° Y-section subcomponents (Initial conditions: $T =$ 550°C, $F = 14$ kN)

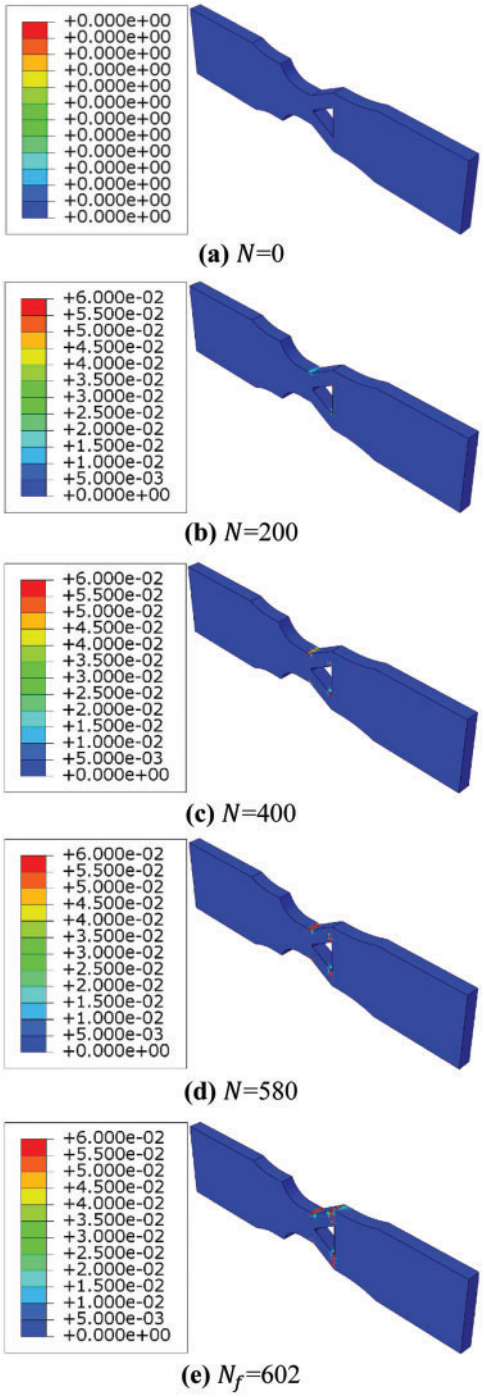

Figure 19: Damage evolution of Ti_2AlNb alloy 60° Y-section subcomponents (Initial conditions: $T =$ 550°C, $F = 14$ kN)

When the improved Lemaitre damage evolution theory is used to predict the fatigue life of subcomponents, the maximum number of failure cycles is far less than expected, but the failure cycle

cannot converge. At this point, stiffness degradation has just begun, so the number of cycles applied at each analysis step needs to be adjusted. In addition, the unscientific division of the FEM grid will also lead to the appearance of some defective data.

4 Conclusion

In this paper, the low cycle fatigue behaviour of Ti_2AlNb alloy Y-section subcomponents has been studied experimentally and numerically. The finite element simulation parameters of Ti_2AlNb alloy standard open-hole specimen were determined based on the fatigue test data. The fatigue life of Ti_2AlNb alloy Y-section subcomponents was predicted, which solved the problem that it was difficult to conduct conventional fatigue tests for complex Ti_2AlNb alloy subcomponents. Some critical conclusions are summarized as follows:

(1) The convergence of the finite element model mesh of Ti_2AlNb alloy standard open-hole specimen was analyzed using fatigue test data at 550°C and 650°C. The optimal global mesh size of the Seeger theory and the improved Lemaitre theory is 2 mm, and the optimal local mesh size is 0.2 and 1 mm, respectively.

(2) The fatigue life of the Ti_2AlNb alloy standard open-hole specimen was predicted. The average error of maximum failure cycles of Ti_2AlNb alloy standard open-hole specimen at 550°C and 650°C between Seeger theory and test is 12.4% and 15.2%, respectively. The nine-point average error between the Seeger theory and the test value is 13.8%. The average error of maximum failure cycles of Ti_2AlNb alloy standard open-hole specimen at 550°C and 650°C between improved Lemaitre damage evolution theory and test is 21.4% and 12.5%, respectively. The stiffness of the grid element degrades rapidly when the cyclic stress is high, resulting in a significant error at 550°C. The nine-point average error between the improved Lemaitre theory and the test value is 16.9%. The average errors of fatigue life predicted by the Seeger theory and the improved Lemaitre theory are 13.8% and 16.9%, respectively.

(3) The load amplitude, temperature, and Y-interface angle are negatively correlated with the fatigue life of the Ti_2AlNb alloy Y-section subcomponents. The average error of fatigue life of Ti_2AlNb alloy Y-section subcomponents predicted by two theoretical methods is 20.6%. By observing the failure position of the structures, it is found that the increase of the angle of the interface area will amplify the stress concentration effect, thus reducing the fatigue life, which is consistent with the Seeger theory results.

Funding Statement: The authors are grateful for the financial support provided by the National Science and Technology Major Project (No. J2019-VI-0003-0116) and the Six Talent Peaks Project in Jiangsu Province (Grant No. 2019-KTHY-059).

Conflicts of Interest: The authors declare that they have no conflicts of interest to report regarding the present study.

References

1. Kumpfert, J. (2001). Intermetallic alloys based on orthorhombic titanium aluminide. *Advanced Engineering Materials, 3(11),* 851–864. https://doi.org/10.1002/1527-2648(200111)3:11<851::Aid-adem851>3.0.Co;2-g
2. Boehlert, C. J. (2001). Part III. The tensile behavior of Ti-Al-Nb O+Bcc orthorhombic alloys. *Metallurgical and Materials Transactions A, 32(8),* 1977–1988. https://doi.org/10.1007/s11661-001-0010-4

3. Zhou, Y., Wang, D., Song, L., Mukhtar, A., Huang, D. et al. (2021). Effect of heat treatments on the microstructure and mechanical properties of Ti_2AlNb intermetallic fabricated by selective laser melting. *Materials Science and Engineering A, 817*. https://doi.org/10.1016/j.msea.2021.141352
4. Li, Z., Cui, Y., Yu, Z., Liu, C. (2021). In-situ fabrication of Ti_2AlNb-based alloy through double-wire arc additive manufacturing. *Journal of Alloys and Compounds, 876*. https://doi.org/10.1016/j.jallcom.2021.160021
5. Zhang, H., Li, C., Ma, Z., Yu, L., Liu, Y. (2019). Effect of dual aging treatments on phase transformation and microstructure in a pre-deformed Ti_2AlNb-based alloy containing O + β/*B2* structures. *Vacuum, 164,* 175–180. https://doi.org/10.1016/j.vacuum.2019.03.022
6. Huang, Y., Liu, Y., Zhang, Y., Liang, H. (2020). Thermal stability and mechanical properties of Ti-22Al-25Nb alloy with different initial microstructures. *Journal of Alloys and Compounds, 842*. https://doi.org/10.1016/j.jallcom.2020.155794
7. Zheng, Y., Zeng, W., Zhang, P., Ma, H., Li, D. et al. (2020). Anti-correlation between solution strengthening and precipitation strengthening in lamellar O microstructures of a Ti_2AlNb based alloy. *Journal of Alloys and Compounds, 847*. https://doi.org/10.1016/j.jallcom.2020.156470
8. Zhang, H., Zhang, Y., Liang, H., Yu, L., Liu, Y. (2020). Effect of the primary O phase on thermal deformation behavior of a Ti_2AlNb-based alloy. *Journal of Alloys and Compounds, 846*. https://doi.org/10.1016/j.jallcom.2020.156458
9. Dang, W., Li, J., Zhang, T., Kou, H. (2015). Oxidation behavior of Zr-containing Ti_2AlNb-based alloy at 800°C. *Transactions of Nonferrous Metals Society of China, 25(3),* 783–790. https://doi.org/10.1016/s1003-6326(15)63664-0
10. Germann, L., Banerjee, D., Guedou, J. Y., Strudel, J. L. (2005). Effect of composition on the mechanical properties of newly developed Ti_2AlNb-based titanium aluminide. *Intermetallics, 13(9),* 920–924. https://doi.org/10.1016/j.intermet.2004.12.003
11. Du, Z., Ma, S., Han, G., Wei, X., Han, J. et al. (2021). The parameter optimization and mechanical property of the honeycomb structure for Ti_2AlNb based alloy. *Journal of Manufacturing Processes, 65,* 206–213. https://doi.org/10.1016/j.jmapro.2021.03.031
12. Zhang, Y., Cai, Q., Ma, Z., Li, C., Yu, L. et al. (2019). Solution treatment for enhanced hardness in Mo-modified Ti_2AlNb-based alloys. *Journal of Alloys and Compounds, 805,* 1184–1190. https://doi.org/10.1016/j.jallcom.2019.07.149
13. Tang, F., Nakazawa, S., Hagiwara, M. (2002). The effect of quaternary additions on the microstructures and mechanical properties of orthorhombic Ti_2AlNb-based alloys. *Materials Science and Engineering A, 329,* 492–498. https://doi.org/10.1016/s0921-5093(01)01626-4
14. Zhang, H., Zhang, Y., Liang, H., Liu, Y. (2021). Influence of cooling rates on microstructure and tensile properties of a heat treated Ti_2AlNb-based alloy. *Materials Science and Engineering A, 817*. https://doi.org/10.1016/j.msea.2021.141345
15. Bu, Z., Zhang, Y., Yang, L., Kang, J., Li, J. (2022). Effect of cooling rate on phase transformation in Ti_2AlNb alloy. *Journal of Alloys and Compounds, 893*. https://doi.org/10.1016/j.jallcom.2021.162364
16. Chen, Y., Wang, J., Gao, Y., Feng, A. (2019). Effect of shot peening on fatigue performance of Ti_2AlNb intermetallic alloy. *International Journal of Fatigue, 127,* 53–57. https://doi.org/10.1016/j.ijfatigue.2019.05.034
17. Fu, Y., Lv, M., Zhao, Q., Zhang, H., Cui, Z. (2021). Investigation on the size and distribution effects of O phase on fracture properties of Ti_2AlNb superalloy by using image-based crystal plasticity modeling. *Materials Science and Engineering A, 805*. https://doi.org/10.1016/j.msea.2021.140787
18. Chen, Y., Gao, Y. (2019). Simulation of the residual stress and fatigue prediction of Ti_2AlNb intermetallic compound under shot peening. *Surface Technology, 48,* 167–172+188. https://doi.org/10.16490/j.cnki.issn.1001-3660.2019.06.019
19. Basquin, O. (1910). The exponential law of endurance tests. *Proceedings-American Society for Testing and Materials,* vol. 10, pp. 625–630.

20. Morrow, J. (1965). Cyclic plastic strain energy and fatigue of metals. *ASTM,* 45–87. https://doi.org/10.1520/STP378-EB
21. Coffin, L. (1954). A study of the effects of cyclic thermal stresses on a ductile metal. *Transactions of the American Society of Mechanical Engineers, 76(6),* 931–949. https://doi.org/10.1115/1.4015020
22. Morrow, J., Raske, D. (1969). *Mechanics of materials in low cycle fatigue testing*. Dordrecht, Netherlands: Kluwer Academic Publishers-Plenum Publishers.
23. Zhang, Y., Chen, Z., Qu, S., Feng, A., Mi, G. et al. (2020). Microstructure and cyclic deformation behavior of a 3D-printed Ti-6Al-4 V alloy. *Journal of Alloys and Compounds, 825*. https://doi.org/10.1016/j.jallcom.2020.153971
24. Smith, K., Watson, P., Topper, T. (1970). A stress-strain functions for the fatigue of metals (stress-strain function for metal fatigue including mean stress effect). *Journal of Materials Science & Technology, 5,* 767–778.
25. Lorenzo, F., Laird, C. (1984). A new approach to predicting fatigue life behavior under action of mean stresses. *Materials Science and Engineering A, 62,* 205–210. https://doi.org/10.1016/0025-5416(84)90223-4
26. Ince, A., Glinka, G. (2014). A generalized fatigue damage parameter for multiaxial fatigue life prediction under proportional and non-proportional loadings. *International Journal of Fatigue, 62,* 34–41. https://doi.org/10.1016/j.ijfatigue.2013.10.007
27. Bäumel, A., Seeger, T., Boller, C. (1987). *Materials data for cyclic loading*. Amsterdam, Netherlands: Elsevier Science Publishers.
28. Lemaitre, J. (1996). *A course on damage mechanics*. Berlin, Germany: Springer-Verlag.
29. Ellyson, B., Chekir, N., Brochu, M. (2017). Characterization of bending vibration fatigue of WBD fabricated Ti-6A1-4 V. *International Journal of Fatigue, 101,* 36–44. https://doi.org/10.1016/j.ijfatigue.2017.03.045
30. Long, X., Guo, Y., Su, Y., Siow, K. S., Chen, C. (2022). Constitutive, creep, and fatigue behavior of sintered Ag for finite element simulation of mechanical reliability: A critical review. *Journal of Materials Science: Materials in Electronics, 33(5),* 2293–2309. https://doi.org/10.1007/s10854-021-07474-1
31. Yang, B., Luo, J., Wan, B., Su, Y., Fu, G. et al. (2022). Numerical and experimental investigations of the thermal fatigue lifetime of CBGA packages. *Computer Modeling in Engineering & Sciences, 130(2),* 1113–1134. https://doi.org/10.32604/cmes.2022.018037
32. Zhou, S., Liu, J., Huang, B. (2008). Continuum damage mechanics study on low-cycle fatigue damage of Ti alloy TC4. *Journal of Mechanical Strength, 30,* 798–803. https://doi.org/10.16579/j.issn.1001.9669.2008.05.009
33. Song, S., Han, Y., Xu, L. (2019). The research of low cycle fatigue damage of Ti-6Al-4 V titanium alloy based on combined hardening model. *Transactions of the China Welding Institution, 40,* 43–48. https://doi.org/10.12073/j.hjxb.2019400009
34. Yang, S., Yang, L., Wang, Y. (2020). Determining the fatigue parameters in total strain life equation of a material based on monotonic tensile mechanical properties. *Engineering Fracture Mechanics, 226*. https://doi.org/10.1016/j.engfracmech.2019.106866
35. Jing, H., Pan, S., Xu, L., Zhao, L., Han, Y. (2021). Bending fatigue behavior and damage mechanism of the Ti-6Al-4 V titanium alloy. *Journal of Tianjin University: Natural Science & Engineering Technology, 54,* 942–949. https://doi.org/10.11784/tdxbz202006023
36. Poursan Dalir, M., Hedayati, E., Hedayati, A. (2021). Detection and identification of subcutaneous defects using ultrasonic waves in reflective test. *Journal of Mechanical Engineering and Sciences, 15(2),* 8003–8015. https://doi.org/10.15282/jmes.15.2.2021.06.0631
37. Hedayati, E., Vahedi, M. (2017). Numerical investigation of penetration in Ceramic/Aluminum targets using smoothed particle hydrodynamics method and presenting a modified analytical model. *Computer Modeling in Engineering & Sciences, 113(3),* 295–323. https://doi.org/10.3970/cmes.2017.113.307